Generalized potential theory for close-range acoustic interactions in the Rayleigh limit

Shahrokh Sepehrirhnama and Kian-Meng Lim[*]

Mechanical Engineering Department, National University of Singapore, Singapore 117575

Under an external acoustic field, particles experience radiation forces that bring them to certain trapping locations, such as pressure or velocity nodes for the case of plane standing wave. Due to acoustical interactions, particles form clusters on reaching those trapping locations. In this work, by using the far-field evaluation of scattered fields, a generalized force potential is formulated that gives both the primary and interaction forces for particles with size much smaller than the wavelength (Rayleigh limit). The generalized potential for the primary force is the same as the Gorkov's potential. The interaction potential and forces between a pair of particles at the zero-primary-force locations are studied for the two cases of planar and nonplanar (Bessel) standing waves. It was found that the interaction forces are predominantly dependent on the product of the external acoustic field and the scattered fields from the adjacent particles. Besides the line formation, other cluster shapes are shown to be plausible for three solid particles agglomerating under a plane standing wave. The mutual interaction force between particles of different material properties was found to be not equal and opposite in general, suggesting that they do not form an action and reaction pair. From the interaction patterns due to the nonplanar field of a Bessel standing wave, it is inferred that many cluster configurations are possible since particles near the stable trapping locations attract each other from more than one direction. The advantage of using the generalized force potential is that it provides physical insight for the acoustical manipulation of small particles in any external field with arbitrary wave front, such as those used in acoustic holography.

I. INTRODUCTION

Ultrasound manipulation of particles relies on the acoustic radiation forces that is exerted on each individual particle that scatters the external sound field [1–5]. Acoustic radiation forces have two distinct types. The first one is usually referred to as the primary radiation force and originates from the nonlinear stresses entirely due to the external pressure field [1–3,5–14]. The second type is the so-called secondary radiaiton force that arises from the stresses due to cross-product of background field and scattered fields of neighboring objects incident on the target particle. Hence, the secondary force is commonly regarded as an indicator of the interaction between particles, and alternatively called the acoustic interaction force, and only exists for more than two particles in the sound field [4,11,15–25].

In the applications of the ultrasound particle manipulation, also known as acoustophoresis, agglomeration is highly likely to occur, specially when the interparticle distances are comparable to their characteristic size, since the acoustic interaction force is inversely proportional to the interparticle distance. Such agglomerations could occur during the particles' journey toward or on arriving at the trapping locations, such as nodal planes in a plane standing wave. At the vicinity of the trapping locations where the primary force is negligible, the entire dynamics of the particle system is determined by the secondary forces. Hence, understanding acoustical interaction patterns is imperative to analyze, describe, and potentially control such agglomerations under different types of external sound fields.

Acoustical interaction under plane standing wave has been reported extensively [4,11,15–20,23,26]. In the view of recent studies of acoustic Bessel beams and their pull-in effects on particles of size larger than the wavelength [12,27–29], it is interesting to examine the changes in acoustical interaction patterns under such nonplanar fields. Furthermore, manipulation of the external sound field in applications such as acoustic holography [30] will allow controlling particle agglomeration behavior to some extent. Thus, a simple and straightforward theoretical formulation of acoustic interaction forces that allows predicting complicated interactions under an arbitrary nonplanar incident field is important for developing novel acoustophoresis applications.

There are two analytical approaches for calculating the radiation forces. Following the work of King [1], the first one is based on using the partial-wave expansion, also known as the multipole expansion, for solving the scattering problem and evaluating the surface integral to derive a series expression for the radiation forces. The second approach, introduced by Gorkov, was based on the far-field evaluation of the force integral by employing the conservation of the radiated momentum [3]. In this approach, the force is expressed as the gradient of a scalar potential field. The two approaches will give the same formula for the primary radiation force. The interaction force was studied by using the first approach in the form of a series expansion [16,18,20]. Attempts were made to find an analytical formula for the interaction force, similarly to the one for the primary force, by using the second approach [19].

*limkm@nus.edu.sg

However, there was a large discrepancy, around 50%, between its results and those obtained by the first approach [23]. The main reason for such difference is addressed in this work and by combining the two approaches a more comprehensive derivation will be presented.

In many practical acoustophoretic applications, the particle size is much smaller than the wavelength [17,23,26,31–36]. This size condition is also referred to as the Rayleigh limit, at which the scattering behavior of particles can be accurately estimated by monopole-dipole scattering fields. For a particle in the Rayleigh limit with arbitrary shape, the acoustic radiation forces can be fairly estimated by using an equivalent sphere with the same volume. Furthermore, hundreds or thousands of such small particles are present in practical applications, even though the occupied volume of their population is much smaller, as compared to the host fluid. This means close-range interactions are very likely to occur during ultrasound manipulation; it is more sensible to use multiparticle interaction model rather than single-particle analysis to simulate their collective behavior.

In this work, the theory of acoustic radiation force is revisited. Following Gorkov's approach, a generalized force potential is introduced from which the expressions for the primary and secondary radiation forces are derived. To focus on the overall interaction patterns, we assume that the host fluid is lossless and hydrodynamic effects of the acoustic streaming are negligible. The force potential is used to investigate the radiation forces induced by standing waves of plane and Bessel types. Subsequently, particle interaction under each of these external fields is discussed by using the force potential and its gradient. We aim to demonstrate how the interaction patterns depend on particles' material, size, and the choice of the external field by using the generalized potential. This will provide a better physical insight for designing particle manipulation processes by using ultrasound waves. The presented formulation can be further developed for the case of nonspherical particles and study of acoustic radiation torque.

II. POTENTIAL THEORY OF ACOUSTIC RADIATION FORCE

The governing equation of acoustic waves, derived from the first-order approximation of Navier-Stokes equations, is expressed as

$$\nabla^2 p = \frac{1}{c_f^2} \partial_t^2 p, \qquad (1)$$

where p is the acoustic pressure. The acoustic velocity $\mathbf{v}$, density ρ, velocity potential ϕ, and their relations to the pressure are as follows:

$$\mathbf{v} = \nabla \phi, \quad p = -\rho_f \partial_t \phi,$$
$$\partial_t \rho = -\rho_f \nabla \cdot \mathbf{v}, \quad p = c_f^2 \rho, \qquad (2)$$

where ∂_t denotes partial differentiation with respect to time t, c_f denotes the speed of sound in the fluid medium, ρ_f and κ_f are the undisturbed fluid density and compressibility, respectively, and $c_f^2 = 1/(\rho_f \kappa_f)$. The acoustic fields are assumed to be time harmonic,

$$\mathbf{v} = \mathbf{V} e^{-i\omega t}, \quad p = P e^{-i\omega t}, \quad \phi = \Phi e^{-i\omega t}, \qquad (3)$$

with ω being the circular frequency and $i = \sqrt{-1}$.

A. Acoustic radiation force

By neglecting the viscosity of the fluid medium, the time-averaged second-order acoustic stresses $\langle \boldsymbol{\sigma} \rangle$ are expressed as follows [5,7]:

$$\langle \boldsymbol{\sigma} \rangle = \left[\tfrac{1}{2} \kappa_f \langle p^2 \rangle - \tfrac{1}{2} \rho_f \langle \mathbf{v} \cdot \mathbf{v} \rangle \right] \mathbf{I} + \rho_f \langle \mathbf{v}\mathbf{v} \rangle, \qquad (4)$$

where $\mathbf{I}$ is the identity tensor. The acoustic radiation force acting on an object in the sound field is obtained as follows:

$$\mathbf{F} = -\int_\Gamma \langle \boldsymbol{\sigma} \rangle \cdot \mathbf{n} d\Gamma = -\int_\Gamma \left\{ \left[\frac{1}{2} \kappa_f \langle p^2 \rangle - \frac{1}{2} \rho_f \langle \mathbf{v} \cdot \mathbf{v} \rangle \right] \mathbf{I} \right.$$
$$\left. + \rho_f \langle \mathbf{v}\mathbf{v} \rangle \right\} \cdot \mathbf{n} d\Gamma, \qquad (5)$$

where Γ is the surface of the object and $\mathbf{n}$ is the outward normal vector to surface Γ. The time-averaging over one cycle of oscillation is denoted by $\langle \cdot \rangle$, and $\langle \mathscr{F}\mathscr{G} \rangle = \tfrac{1}{2}\text{Re}[\mathscr{F}\mathscr{G}^*]$ with * denoting the complex conjugate operator. The first two terms on the right-hand side of Eq. (4) are commonly known as the radiation pressure that is derived from the second-order approximation of Navier-Stokes equations [5,37]. The last term represents the Reynolds stress that arises from the surface oscillations [5]. The velocity potential, for the case of N-body scattering and an external acoustic wave, is written as

$$\phi = \phi_0 + \sum_{n=1}^{N} \phi_n, \qquad (6)$$

where subscript 0 denotes the external field and n denotes the scattered field from the nth object. Substituting Eq. (6) into (4), the quadratic terms can be expanded in terms of incident and scattered variables, for instance,

$$p^2 = p_0 p_0 + \sum_{n=1}^{N} p_n p_n + \sum_{n=1}^{N} p_n \left(2p_0 + \sum_{\substack{m=1 \\ m \neq n}}^{N} p_m \right). \qquad (7)$$

The product or cross-term of the external field with itself, such as $p_0 p_0$ from Eq. (7) and similar terms from the expansions of $\langle \mathbf{v} \cdot \mathbf{v} \rangle$ and $\langle \mathbf{v}\mathbf{v} \rangle$, do not contribute to the force as the external field has no singularity in the domain [7,18,37]. The force due to the cross-term of the scattered field from the target particle itself $\langle p_n p_n \rangle$ is negligible in the Rayleigh limit, since it has been shown to be of the order of $\mathcal{O}([ka]^6)$, while the rest of the acoustic forces are of the order of $\mathcal{O}([ka]^3)$ [1,3,8,37]. Considering the remaining terms in Eq. (7), the partial stresses obtained from the product of incident field and the scattered field of sphere n becomes

$$\langle \boldsymbol{\sigma}_n \rangle = [\kappa_f \langle p_n \hat{p}_n \rangle - \rho_f \langle \mathbf{v}_n \cdot \hat{\mathbf{v}}_n \rangle]\mathbf{I} + 2\rho_f \langle \mathbf{v}_n \hat{\mathbf{v}}_n \rangle$$
$$\hat{p}_n = p_0 + \sum_{\substack{m=1 \\ m \neq n}}^{N} p_m \quad \hat{\mathbf{v}}_n = \mathbf{v}_0 + \sum_{\substack{m=1 \\ m \neq n}}^{N} \mathbf{v}_m, \qquad (8)$$

where $\hat{p}_n$ and $\hat{\mathbf{v}}_n$ denote the incident pressure and velocity on sphere n that consist of the sum of the external field and the scattered fields from other particles ($m \neq n$). Adopting the far-field approach [3,19,37], the force acting on sphere n is
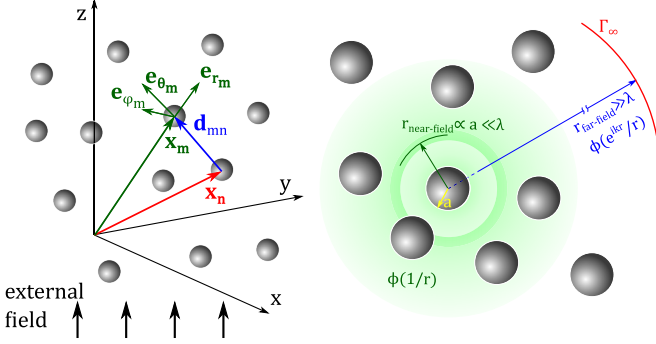
FIG. 1. Ensemble of N particles in an external acoustic field and the illustration of near-field and far-field regions.

written as

$$\mathbf{F}_n = -\int_{\Gamma_\infty} \langle \boldsymbol{\sigma}_n \rangle \cdot \mathbf{n} d\Gamma. \quad (9)$$

By substituting Eq. (8) into (9), applying the divergence theorem to transform the surface integral into a volume integral, and using the relation between acoustic fields as stated in Eq. (2), one can write

$$\mathbf{F}_n = -\int_\Omega \rho_f \{ \langle \hat{\mathbf{v}}_n \Box \phi_n \rangle + \langle \mathbf{v}_n \Box \hat{\phi}_n \rangle \} d\Omega, \quad (10)$$

where $\Box = \nabla^2 - \frac{1}{c_f^2} \partial_t^2$ denotes the wave operator and Ω denotes the volume that is enclosed by Γ_∞. For the derivation details of Eq. (10) from (9), please refer to Eqs. (13a) to (13f) in Ref. [37]. When we consider the force on individual spheres one after another, the singularity of the scattered field ϕ_n needs to be handled only while calculating the force on sphere n. For the calculation of the force on sphere n, the incident field $\hat{\phi}_n$ is regular everywhere and $\Box \hat{\phi}_n = 0$. Then Eq. (10) becomes

$$\mathbf{F}_n = -\int_\Omega \rho_f \langle \hat{\mathbf{v}}_n \Box \phi_n \rangle d\Omega$$

$$= -\int_\Omega \rho_f \left\langle \mathbf{v}_0 \Box \phi_n + \sum_{\substack{m=1 \\ m \neq n}}^N \mathbf{v}_m \Box \phi_n \right\rangle d\Omega, \quad (11)$$

From the first-order scattering theory [3,8,37], the far-field approximation of the scattered potential ϕ_n in terms of the acoustic density $\hat{\rho}_n$ and velocity $\hat{\mathbf{v}}_n$ fields incident on the nth particle is written as follows:

$$\phi_n = -\alpha_n \frac{a_n^3}{3\rho_f} \partial_t \hat{\rho}_n \frac{e^{ikr_n}}{r_n} - \frac{\beta_n}{2} a_n^3 \nabla \cdot \left(\hat{\mathbf{v}}_n \frac{e^{ikr_n}}{r_n} \right),$$

$$\hat{\rho}_n = \rho_0 + \sum_{\substack{m=1 \\ m \neq n}}^N \rho_m \quad \hat{\mathbf{v}}_n = \mathbf{v}_0 + \sum_{\substack{m=1 \\ m \neq n}}^N \mathbf{v}_m, \quad (12)$$

where r_n is the radial distance from the center of sphere n (with radius a_n) located at $\mathbf{x}_n$, as shown in Fig. 1. The terms α_n and β_n denote monopole and dipole coefficients, respectively, associated with sphere n. By applying the wave operator, Eq. (12) gives

$$\Box \phi_n = \alpha_n \frac{4\pi a_n^3}{3\rho_f} \partial_t \hat{\rho}_n \delta(r_n) + \beta_n 2\pi a_n^3 \nabla \cdot (\hat{\mathbf{v}}_n \delta(r_n))$$

$$n = 1, 2, \ldots, N, \quad (13)$$

where δ denotes the Dirac delta function. The acoustic sources of order $\mathcal{O}(r_n^{-3})$ and beyond are neglected in the far-field approximation. By using Eq. (13), the volume integral in Eq. (10) reduces to

$$\mathbf{F}_n = 2\pi a_n^3 \rho_f \langle \beta_n \hat{\mathbf{v}}_n \cdot \nabla \hat{\mathbf{v}}_n \rangle_{\mathbf{x}=\mathbf{x}_n} - \frac{4\pi a_n^3}{3} \langle \alpha_n \hat{\mathbf{v}}_n \partial_t \hat{\rho}_n \rangle_{\mathbf{x}=\mathbf{x}_n}, \quad (14)$$

which can be further simplified by using $\langle \mathcal{F} \partial_t \mathcal{G} \rangle = -\langle \mathcal{G} \partial_t \mathcal{F} \rangle$ and $\nabla \hat{p}_n = -\rho_f \partial_t \hat{\mathbf{v}}_n$, to give

$$\mathbf{F}_n = 2\pi a_n^3 \rho_f \langle \beta_n \hat{\mathbf{v}}_n \cdot \nabla \hat{\mathbf{v}}_n \rangle_{\mathbf{x}=\mathbf{x}_n} - \frac{4\pi a_n^3}{3} \kappa_f \langle \alpha_n \hat{p}_n \nabla \hat{p}_n \rangle_{\mathbf{x}=\mathbf{x}_n}. \quad (15)$$

For the derivation details of Eq. (15) from (11), please see Eqs. (14) to (15d) from Ref. [37]. Finally, $\mathbf{F}_n$ can be expressed as the gradient of the generalized potential by factoring out the gradient operator in Eq. (15), as follows:

$$\mathbf{F}_n = -\nabla G_n(\mathbf{x}_n)$$

$$G_n = \Omega_n \left[\frac{\kappa_f}{2} \langle \alpha_n \hat{p}_n \hat{p}_n \rangle - \frac{3\rho_f}{4} \langle \beta_n \hat{\mathbf{v}}_n \cdot \hat{\mathbf{v}}_n \rangle \right], \quad (16)$$

where G_n denotes the generalized potential associated with sphere n and $\Omega_n = \frac{4\pi a_n^3}{3}$ denote the volume of the target sphere n.

B. Primary and secondary radiation forces and potentials

One may attempt to split the force acting on sphere n into the primary force and secondary force (or interaction force). We expand the product term as follows:

$$\hat{p}_n \nabla \hat{p}_n = \left(p_0 + \sum_{\substack{m=1 \\ m \neq n}}^N p_m \right) \nabla \left(p_0 + \sum_{\substack{l=1 \\ l \neq n}}^N p_l \right) = p_0 \nabla p_0 + p_0 \sum_{\substack{l=1 \\ l \neq n}}^N \nabla p_l + \sum_{\substack{m=1 \\ m \neq n}}^N p_m \nabla p_0 + \left(\sum_{\substack{m=1 \\ m \neq n}}^N p_m \right) \left(\sum_{\substack{l=1 \\ l \neq n}}^N \nabla p_l \right)$$

$$= p_0 \nabla p_0 + \nabla \left(p_0 \sum_{\substack{m=1 \\ m \neq n}}^N p_m \right) + \sum_{\substack{m=1 \\ m \neq n}}^N \left[p_m \nabla p_m + \sum_{\substack{l=1 \\ l \neq n, l > m}}^N (p_m \nabla p_l + p_l \nabla p_m) \right]$$

$$= p_0 \nabla p_0 + \sum_{\substack{m=1 \\ m \neq n}}^{N} \nabla (p_0 p_m) + \sum_{\substack{m=1 \\ m \neq n}}^{N} \left[p_m \nabla p_m + \frac{1}{2} \sum_{\substack{l=1 \\ l \neq m,n}}^{N} \nabla (p_m p_l) \right]. \tag{17}$$

The second and third terms in the second line are combined to form the second term in the third line, and the last term in the second line is expanded to isolate the self-interaction term $p_m \nabla p_m$. Applying a similar expansion to the velocity product term, we split the total force acting on sphere n into two parts:

$$\mathbf{F}_n = \mathbf{F}_n^0 + \sum_{\substack{m=1 \\ m \neq n}}^{N} \mathbf{F}_n^m, \tag{18}$$

$$\mathbf{F}_n^0 = 2\pi a_n^3 \rho_f \langle \beta_n \mathbf{v}_0 \cdot \nabla \mathbf{v}_0 \rangle_{\mathbf{x}=\mathbf{x}_n} - \frac{4\pi a_n^3}{3} \langle \alpha_n p_0 \nabla p_0 \rangle_{\mathbf{x}=\mathbf{x}_n}, \tag{19}$$

$$\mathbf{F}_n^m = 2\pi a_n^3 \rho_f \left\langle \beta_n \left[\nabla (\mathbf{v}_m \cdot \mathbf{v}_0) + \mathbf{v}_m \cdot \nabla \mathbf{v}_m + \frac{1}{2} \sum_{\substack{l=1 \\ l \neq m,n}}^{N} \nabla (\mathbf{v}_m \cdot \mathbf{v}_l) \right] \right\rangle_{\mathbf{x}=\mathbf{x}_n}$$

$$- \frac{4\pi a_n^3}{3} \left\langle \alpha_n \left[\nabla (p_0 p_m) + p_m \nabla p_m + \frac{1}{2} \sum_{\substack{l=1 \\ l \neq m,n}}^{N} \nabla (p_m p_l) \right] \right\rangle_{\mathbf{x}=\mathbf{x}_n}, \tag{20}$$

where $\mathbf{F}_n^0$ denotes the primary radiation force that is expressed entirely in terms of the external field (p_0 and $\mathbf{v}_0$), according to Gorkov's theory, and $\sum_{\substack{m=1 \\ m \neq n}}^{N} \mathbf{F}_n^m$ denotes the interaction force acting on sphere n. We have isolated the partial force terms F_n^m that can be attributed to the product of the external field and scattered field of sphere m [for example, $\nabla (p_0 p_m)$]. However, the last term in the expression for F_n^m with sum of terms over the other spheres indicates that this partial force is actually coupled with all spheres present in the system. Finally, the primary and secondary forces are expressed as the negative of the gradient of potential fields, as follows:

$$\mathbf{F}_n^0 = -\nabla G_n^0 \quad G_n^0 = \Omega_n \left\langle \frac{\kappa_f}{2} \alpha_n p_0^2 - \frac{3}{4} \rho_f \beta_n v_0^2 \right\rangle,$$

$$\mathbf{F}_n^m = -\nabla G_n^m \quad G_n^m = \Omega_n \left\langle \kappa_f \alpha_n \left(p_m p_0 + \frac{1}{2} p_m^2 + \frac{1}{2} \sum_{\substack{l=1 \\ l \neq m,n}}^{N} p_m p_l \right) - \frac{3}{2} \rho_f \beta_n \left(\mathbf{v}_m \cdot \mathbf{v}_0 + \frac{1}{2} v_m^2 + \frac{1}{2} \sum_{\substack{l=1 \\ l \neq m,n}}^{N} \mathbf{v}_m \cdot \mathbf{v}_l \right) \right\rangle, \tag{21}$$

where G_n^0 denotes the primary force potential that is actually the Gorkov's potential. The partial interaction potential, denoted by G_n^m, depends on the external and scattered fields from other spheres, and α_n and β_n, which are the monopole and dipole scattering coefficients of the target sphere n. The main advantage of the presented formulation is that the acoustic radiation forces are evaluated directly from the solution of the multibody scattering problem for a given external pressure field p_0.

C. Multibody scattering at Rayleigh limit $ka \ll 1$

Using the partial-wave expansion of the velocity potentials up to dipole around the center of sphere n,

$$\phi_0 = e^{-i\omega t} \sum_{\nu,\mu=0}^{1} A_{\nu\mu}^{(n)} j_\nu (kr_n) Y_\nu^\mu (\theta_n, \varphi_n)$$

$$\phi_n = e^{-i\omega t} \sum_{\nu,\mu=0}^{1} B_{\nu\mu}^{(n)} h_\nu (kr_n) Y_\nu^\mu (\theta_n, \varphi_n)$$

$$\overline{\phi_n} = e^{-i\omega t} \sum_{\nu,\mu=0}^{1} C_{\nu\mu}^{(n)} j_\nu (k_n r_n) Y_\nu^\mu (\theta_n, \varphi_n), \tag{22}$$

where $\sum_{\nu,\mu=0}^{1} = \sum_{\nu=0}^{1} \sum_{\mu=-\nu}^{\nu}$, $(r_n, \theta_n, \varphi_n)$ are the spherical coordinates with respect to the center of sphere n; $\overline{\phi_n}$ denote the refracted velocity potential inside the particle with k_n being the wave number inside the volume of sphere n; $A_{\nu\mu}^{(n)}$, $B_{\nu\mu}^{(n)}$, and $C_{\nu\mu}^{(n)}$ are constant coefficients; and j_ν and h_ν denote spherical Bessel function and Hankel function of the first kind, respectively. Y_ν^μ denotes spherical harmonics that is expressed as follows:

$$Y_\nu^\mu (\theta_n, \varphi_n) = \sqrt{\frac{2\nu+1}{4\pi}} \sqrt{\frac{(\nu-\mu)!}{(\nu+\mu)!}} Q_\nu^\mu (\cos \theta_n) e^{i\mu\varphi_n}, \tag{23}$$

where Q_ν^μ is the associated Legendre polynomials of order ν and degree μ.

The boundary conditions are the continuity of the normal velocity and pressure on the surface of the particles [2], which is written as follows:

$$p_0 + p_n = \overline{p_n}, \quad (\mathbf{v}_0 + \mathbf{v}_n) \cdot \mathbf{n}_n = (\mathbf{u}_n + \overline{\mathbf{v}_n}) \cdot \mathbf{n}_n, \quad (24)$$

where $\mathbf{u}_n$ denotes the rigid-body oscillation velocity and $\mathbf{n}_n$ is the outward normal unit vector to the surface of sphere n. Substituting series expansions from Eq. (22) into (24) and using orthogonal properties of spherical harmonics, the $B_{\nu\mu}$ coefficients are obtained from the following coupled system of equations:

$$\frac{B_{00}^{(n)}}{A_{00}^{(n)} + \mathscr{B}_{00}^{(n)}} = -\frac{\rho_f k_n j_1(k_n a_n) j_0(k a_n) - \rho_n k h_0(k_n a_n) j_1(k a_n)}{\rho_f k_n j_1(k_n a_n) h_0(k a_n) - \rho_n k j_0(k_n a_n) h_1(k a_n)}$$

$$\frac{B_{1\mu}^{(n)}}{A_{1\mu}^{(n)} + \mathscr{B}_{1\mu}^{(n)}} = -\frac{\rho_f k_n j_1'(k_n a_n) j_1(k a_n) - \rho_n k h_1(k_n a_n) j_1'(k a_n)}{\rho_f k_n j_1'(k_n a_n) h_1(k a_n) - \rho_n k j_1(k_n a_n) h_1'(k a_n)}$$

$$\mu = -1, 0, 1, \quad (25)$$

where $\mathscr{B}_{\nu\mu}^{(n)} = \sum_{\substack{m=1 \\ m \neq n}}^{N} \sum_{\overline{\nu\mu}}^{\infty} \mathscr{T}_{\nu\overline{\nu}}^{\mu\overline{\mu}}(k d_{nm}) B_{\overline{\nu\mu}}^{(m)}$ with $\mathscr{T}_{\nu\overline{\nu}}^{\mu\overline{\mu}}$ being the multipole translation operator as given in Eq. (2.8) in Ref. [16].

In Eq. (25), the fraction on left-hand side represents the ratio of scattered field from sphere n over the incident field on it. In the Rayleigh limit, Eq. (25) can be simplified further by using the near-zero asymptotic form of the spherical Bessel and Hankel functions as follows:

$$\frac{B_{00}^{(n)}}{A_{00}^{(n)} + \mathscr{B}_{00}^{(n)}} \approx -i\frac{(k a_n)^3}{3}\left(1 - \frac{\kappa_n}{\kappa_f}\right) = -i\frac{(k a_n)^3}{3}\alpha_n$$

$$\frac{B_{1\mu}^{(n)}}{A_{1\mu}^{(n)} + \mathscr{B}_{1\mu}^{(n)}} \approx i\frac{(k a_n)^3}{6}\left(\frac{2\rho_n - 2\rho_f}{2\rho_n + \rho_f}\right) = i\frac{(k a_n)^3}{6}\beta_n. \quad (26)$$

The monopole coefficient α_n was found to be equal to $1 - \kappa_n/\kappa_f$ by applying the balance between the scattered and incident mass rates [3,37]. The dipole coefficient β_n only depends on the density ratio ρ_n/ρ_f since dipole scattering is related to the rigid-body oscillation [3,37]. While the coefficients α_n and β_n are directly calculated from the ratios of density and speed of sound between fluid and particle, the field coefficients $B_{\nu\mu}^{(n)}$ are coupled through the multipole translation operator $\mathscr{T}_{\nu\overline{\nu}}^{\mu\overline{\mu}}$ that depends on the interparticle distances. The solution of the fully coupled multibody scattering problem is needed to obtain the actual scattered pressure and velocity fields. These scattered fields are subsequently used for evaluating the interaction potential G_n^m, as stated in Eq. (21).

III. RESULTS

In this section, we investigate the interaction patterns under planar and nonplanar standing waves. Zero-order Bessel standing wave (BSW) is considered for studying the effects of nonplanar fields on the interaction forces. It is assumed that the standing waves are in the z direction. We consider spherical polystyrene (PS) beads with $ka = 0.0314 \ll 1$ in water with density ratio of 1.050 and speed-of-sound ratio of

1.567. The results are presented in terms of the normalized potential g and normalized force $\mathbf{S}$, which is a vector quantity. They are expressed as follows:

$$g = \frac{G}{\Omega E_0}, \quad \mathbf{S} = \frac{\mathbf{F}}{\pi a^2 E_0}, \quad \Omega = \sum_{n=1}^{N} \Omega_n, \quad E_0 = \frac{1}{4}\kappa_f |A|^2, \quad (27)$$

where Ω denote the total volume occupied by the system of N particles, E_0 is the acoustic energy density, and A is the pressure magnitude of the external field. We also use the subscripts "pr" and "in," to denote the quantities associated with the primary and interaction forces, respectively, for presenting the results in the this section, instead of the notation used in Sec. II, to avoid numbering the spheres. The normalized force $\mathbf{S}$ is a generalization of the contrast factor that indicates the direction of the acoustic force. Finally, the multibody scattering problem is solved as a coupled system by finding the scattering coefficients $B_{\nu\mu}^{(n)}$ for all the spherical particles simultaneously from Eq. (25) to account for the strong interaction among the spheres when they are placed close to each other.

A. Plane standing wave

The interaction force was calculated by taking the gradient of the corresponding potential, using the central finite-difference method. The results match very well (relative difference of less than 1%) with those obtained from interaction force series in Ref. [16] for two compressible spheres of the same size that are positioned symmetrically on the two sides of the pressure node at interparticle distances $2a$ and $3a$. The plane standing wave with a pressure node at $kz = 0$ was considered for the following numerical investigation.

1. A pair of spheres

The interaction potential between a pair of spheres of the same size is mapped out and presented in Fig. 2. The source sphere is placed on the pressure node $kz = 0$, while the probe sphere is moved over the region of interest. The x-z projection of the potential field within a $4\lambda \times 4\lambda$ region is shown on the left panel. The zero-potential contour lines demonstrate the ripple patterns in the interaction potential at large interparticle distances, implying the change in the force direction. The local maxima and minima occur within the regions between the zero-potential lines. The middle panel shows the potential field in a smaller area of one-wavelength size around the source sphere. The minimum potential occurs on the $kz = 0$ line within the horizontal and narrow strip with darker blue shade. This one-wavelength area is of particular interest since, in some practical acoustophoresis applications, particle manipulation is performed around a single pressure nodal plane within the fluid domain [32–34,38,39].

The interaction potential within a four-radius area is shown on the right panel of Fig. 2. The absolute maximum of the interaction potential occurs at the poles of the source sphere along the kz axis. Since the interaction force acts in the opposite direction of the potential gradient, as stated in Eq. (21), the target sphere is repelled by the source sphere if it approaches these polar regions. Around the equator, the source
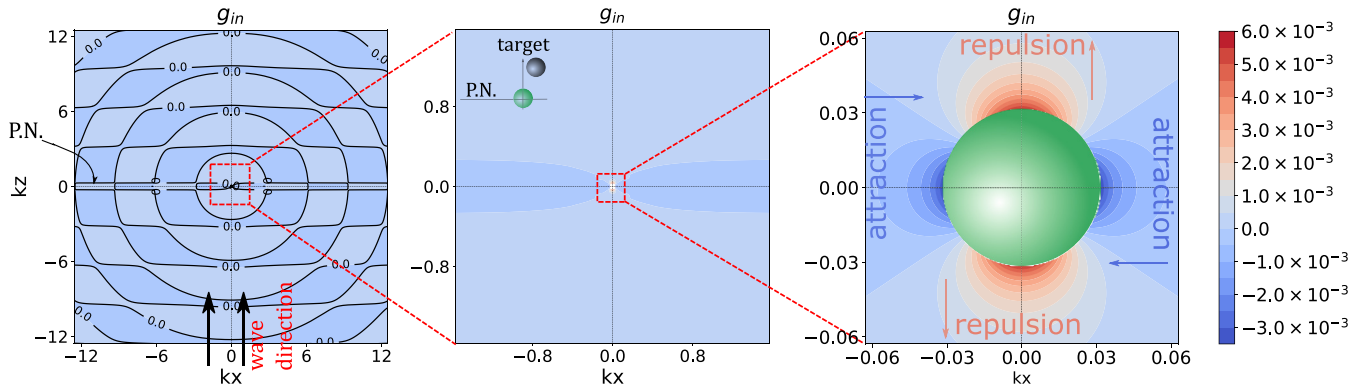
FIG. 2. The normalized interaction potential g_{in} in the x-z plane for a sphere pair with the same size and the source sphere located at the origin of the coordinate system on the pressure nodal plane, denoted by P.N.

sphere attracts the probe sphere, which results in forming a dumbbell-shaped configuration on the pressure nodal plane. This interaction behavior has been widely accepted as the theoretical explanation of the pearl-chain agglomeration pattern, observed in some of the particle-separation applications [32].

From Eq. (21), the partial interaction potential G_n^m can be split into three parts, based on the subscripts that corresponds to the products of the external field and the scattered fields from the other spheres. We investigate the contribution of these terms to the interaction potential, as shown in Fig. 3.
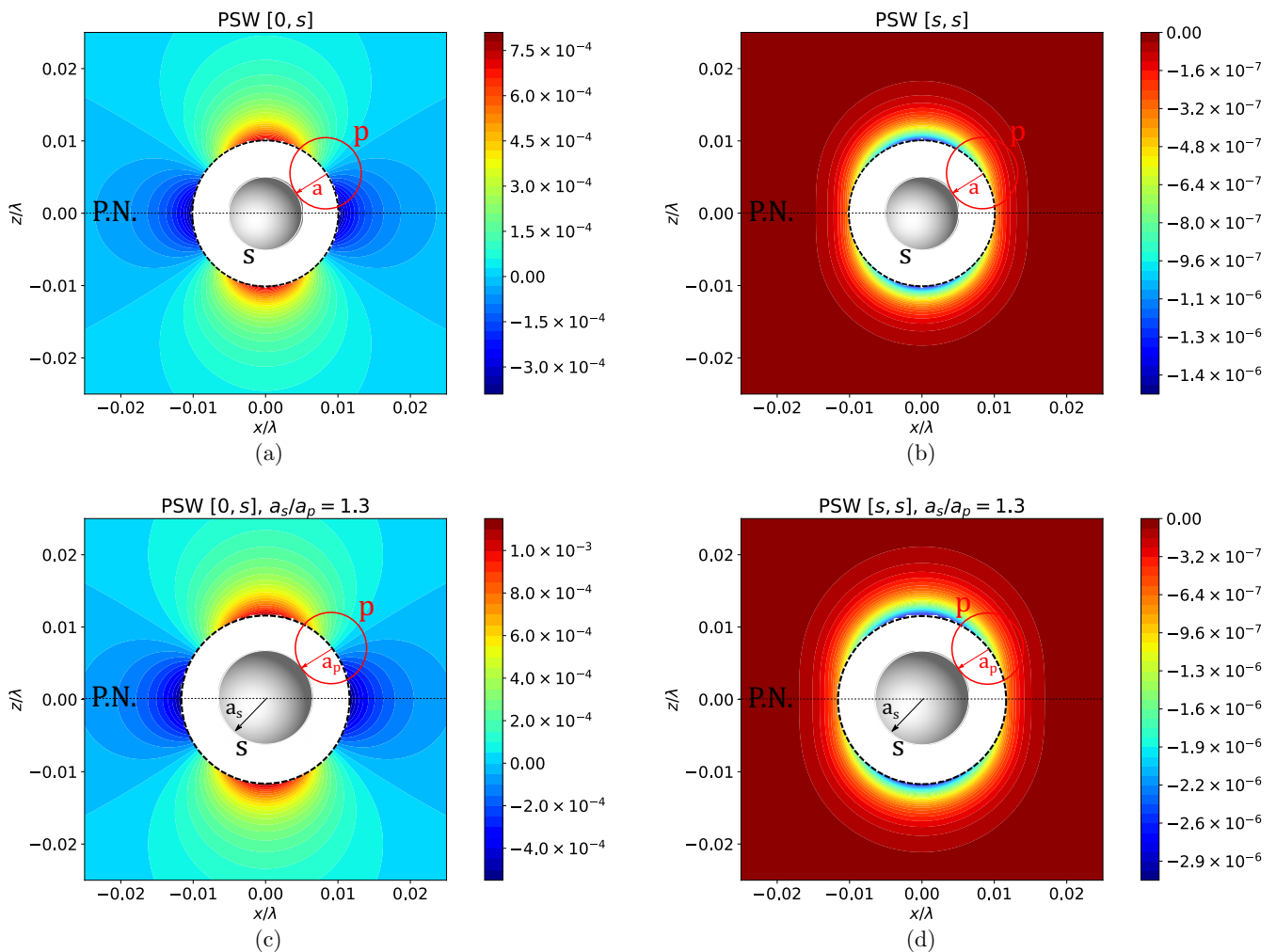

FIG. 3. Projection of the normalized interaction potential g_{in} for the probe sphere on the x-z plane for a pair of spheres under a plane standing wave. Panels (a) and (c) show the contribution from the product of incident field and the scattered field of the source particle, denoted by [0, s], in Eq. (21). The contributions from the self-product term, denoted by [s, s], are shown in panels (b) and (d).
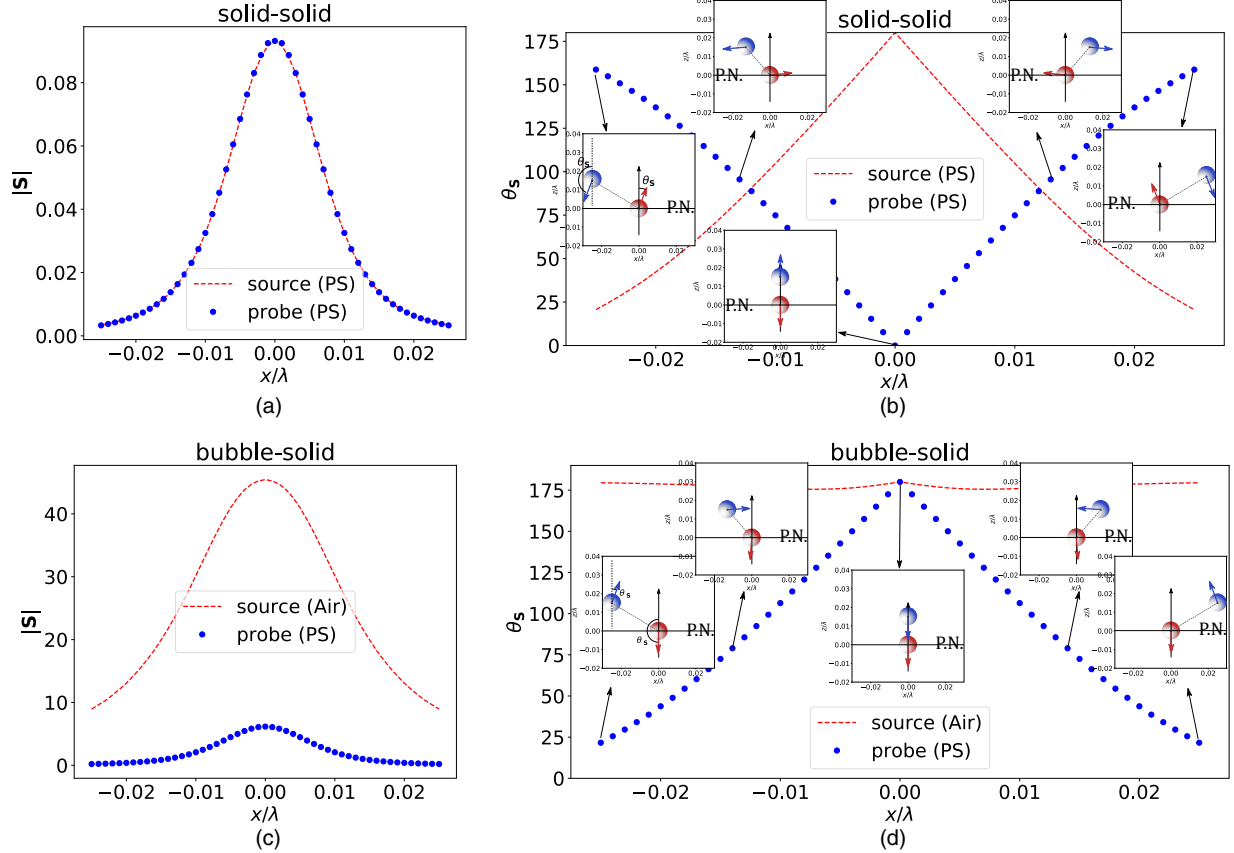
FIG. 4. Magnitude and direction angle of the interaction forces acting on the probe and source spheres, placed in the x-z plane. Panels (a) and (b) show the forces for the case of two solid spheres, while (c) and (d) show the case of solid-bubble interactions. The probe sphere is shifted along a path parallel to the nodal plane at a distance of $3a$ from the plane.

In the case of a pair of spheres with the same radius a, the interaction potential for the probe sphere is evaluated while the source sphere lies on the nodal plane. The contributions of the first part from $p_m p_0$ and $\mathbf{v}_m \cdot \mathbf{v}_0$ terms (denoted by $[0, s]$) and the second part from p_m^2 and v_m^2 terms (denoted by $[s, s]$) in Eq. (21) are shown in Figs. 3(a) and 3(b), respectively. Comparing the range of values, the $[s, s]$ contribution is consistently smaller than that of $[0, s]$ by at least three orders of magnitude. Thus, the second part $[s, s]$ can be neglected without significant loss of accuracy in calculating the interaction potential and forces; hence,

$$G_n^m \approx \Omega_n \langle \kappa_f \alpha_n p_0 p_m - \tfrac{3}{2} \rho_f \beta_n (\mathbf{v}_0 \cdot \mathbf{v}_m) \rangle. \qquad (28)$$

The third part of the interaction potential is only present when there are more than two spheres, and thus it evaluates to zero for this case of two spheres. The same difference between $[0, s]$ and $[s, s]$ parts was observed from Figs. 3(c) and 3(d), when the source sphere has double the volume of the probe sphere, $a_s/a_p \approx 1.3$. This implies that the $[s, s]$ contribution is negligible compared to $[0, s]$ regardless of the relative size of the spheres.

To investigate the mutual acoustic interaction forces, we consider two cases of solid-solid (two PS beads in water) and solid-gas (PS bead and air bubble in water) interactions. In this study, the source sphere is placed at the pressure node, while the probe sphere is moved over a horizontal line along

the x axis from $x = -5a$ to $5a$. The magnitude and polar angle of the normalized forces (denoted by $|\mathbf{S}|$ and θ_S, respectively) are obtained. For the solid-solid case, the interaction forces were found to be equal and opposite, within the accuracy of the numerical calculations, as shown in the first row of Fig. 4. It is inferred that for a homogeneous population of particles of the same material, the interaction forces balances out each other and the resultant force acting on the cluster is the sum of the primary forces. For the case of solid-gas, as shown in the second row of Fig. 4, the mutual interaction forces are distinctly different. The air bubble, used as the source sphere, exhibits a strong monopole scattering, while the scattered field of the PS bead is dominated by dipole scattering. This difference in the scattering patterns accounts for the unequal interaction forces. It was observed that the interaction force acting on the air bubble is larger than the force acting on the PS bead by one to two orders of magnitude. The air bubble is consistently pushed out of the nodal plane along the wave direction, while the force acting on the PS sphere changes direction significantly from $\theta_S = 24°$ to $180°$. When the spheres are along the wave direction, both interaction forces act in the same direction. Hence, the notion that interaction forces being an equal and opposite pair (similarly to Newton's third law) is not valid here. This is due to the break in symmetry in the scattering patterns of two particles of different properties. This implies that the resultant acoustic
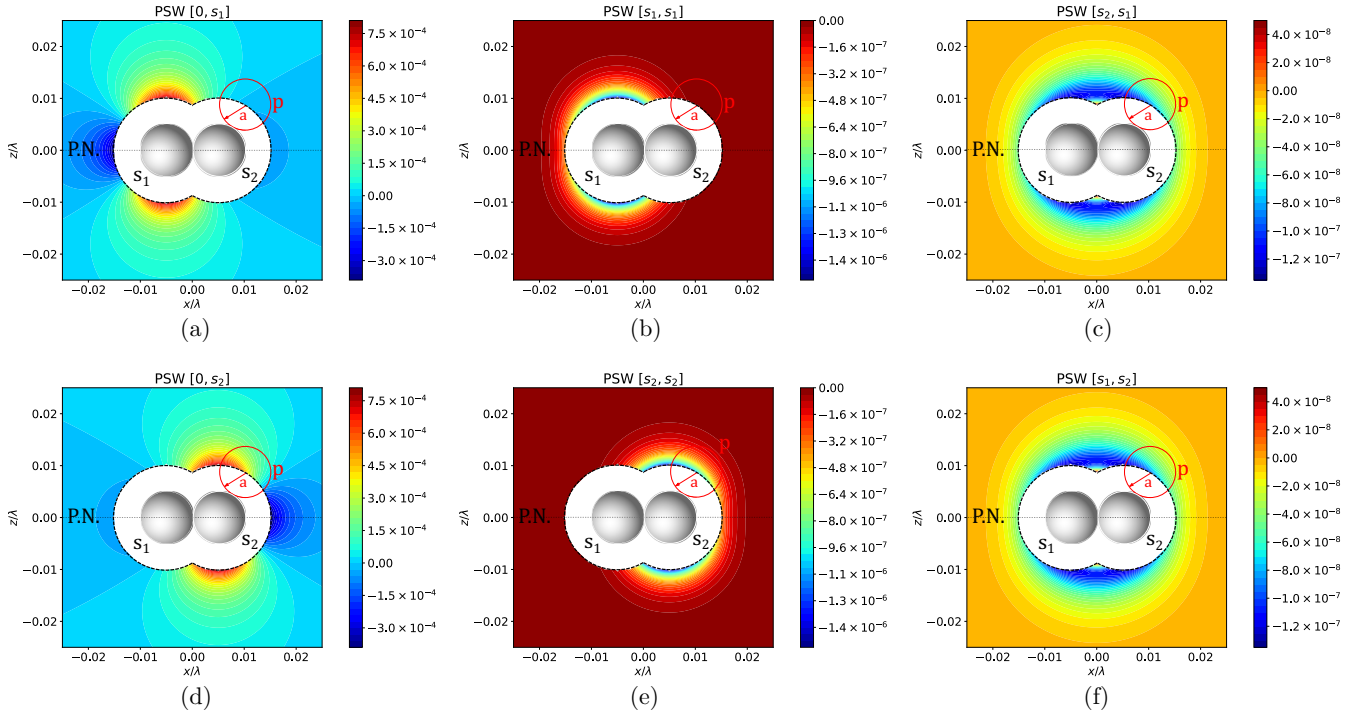
FIG. 5. Projection of the normalized interaction potential g_{in} for the probe sphere on the x-z plane for three spheres with the same size under a plane standing wave. The panels in the last column show the contribution from the cross products of the scattering fields from the two source spheres, denoted by $[s_1, s_2]$ and $[s_2, s_1]$, to the partial interaction potential due to each source sphere, as expressed in Eq. (21).

interaction acting on a heterogeneous population of particles is generally nonzero, and the interactions need to be included in the study of ultrasound particle agglomeration.

2. Three spheres

The interaction potential for the probe sphere due to two source spheres in contact on the nodal plane is shown by parts in Fig. 5. Figures 5(a), 5(b), and 5(c) show the partial interaction potential due to source sphere s_1. It was observed that $[0, s_1]$ contribution is about two to three orders of magnitude larger than the contributions from $[s_1, s_1]$ and $[s_2, s_1]$. Similarly to the case of two spheres, the contributions of the parts with the product of the scattered fields are negligible, and Eq. (28) gives an accurate estimate of the interaction potential for the case of three spheres. Figures 5(c), 5(d), and 5(e) show the results for $[0, s_2]$, $[s_2, s_2]$, and $[s_1, s_2]$. From the similarity between these panels in the two rows, it was concluded that the interaction potential can be studied in a pairwise manner for larger population of particles. Hence, the insights from the study of two spheres are of a great importance to understand the mechanisms of close-range acoustic interactions.

To investigate the agglomeration of particles under plane standing wave (PSW), we use the same case of three spheres. Since the primary force is negligible in the vicinity of the pressure node, the probe sphere is only moved within this region. The interaction force field for this case is shown in Fig. 6. The length of the vectors are normalized while their colors indicate the force magnitude. These normalized vectors S_{in} provide a generalization of the the concept of contrast factor, as they indicate the direction of the interaction force in the

three-dimensional space. In this case where both interacting fields are nonplanar, the interaction force is not one dimensional. The pressure node is shown by a transparent gray plane at $kz = 0$. Three slices of the force field at $y = 0, \pm 5a$, are presented to visualize the spatial behavior of the interaction force field. If the probe sphere is in the same vertical plane $y = 0$ as the source spheres, then it is generally repelled in the z direction and pushed toward either side of the source particles where they form a pearl-chain configuration along the x axis. For the exceptional case of the probe sphere being positioned initially on the z axis and already in contact with the other two, it experiences a strong attraction and is pulled in between the source particles, forming a pearl-chain configuration again. It is noted that when the probe sphere is in the same plane as the source spheres, the interaction force has no out-of-plane component.

When the probe sphere is placed on the planes at $y = \pm 5a$, the z component of the interaction force pushes it toward the pressure node. If the initial position of the probe sphere is far from the pressure node, then the x and y components of the interaction force would push it away from the source spheres while the z component brings it closer to the nodal plane. This will change when the probe sphere gets close to the nodal plane within a threshold distance of about $2.5a$. In this case, the x and y components of the interaction force drive the probe sphere toward the source spheres while the z component continues to bring it toward the nodal plane. Once the probe sphere is on the nodal plane, the z component becomes zero and it moves toward the two source spheres along the nodal plane. In this case, it is possible to see either a triangle or a pearl-chain configuration, depending on direction of approach of the probe sphere.
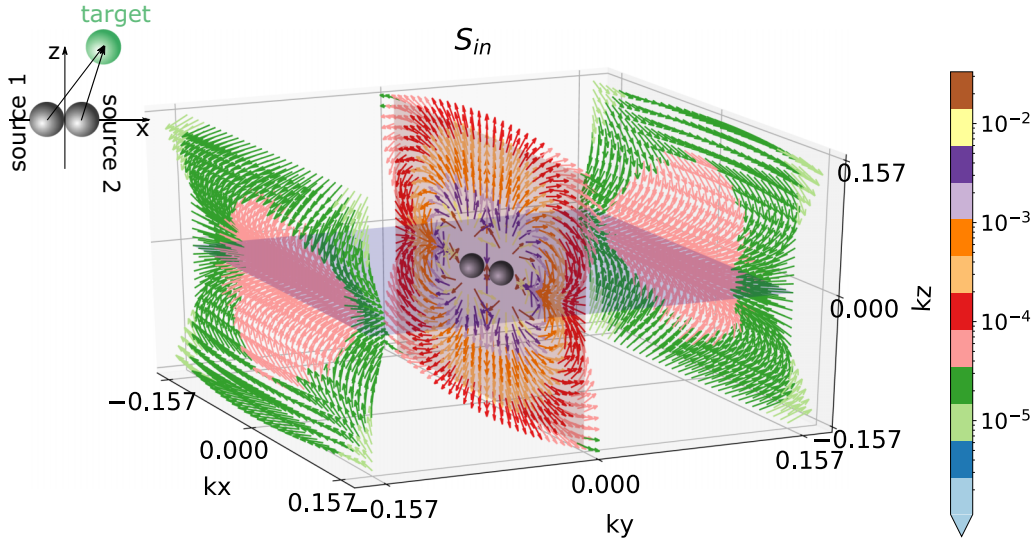
FIG. 6. Contrast factor of the interaction force $\mathbf{S}_{in}$ acting on a target sphere from the two touching source spheres on the pressure nodal plane.

B. Bessel standing wave

A zero-order BSW with its axis being in the z direction and cone angle γ is expressed as follows:

$$p = A J_0(k_R R) \cos(k_z z + \pi/2) e^{-i\omega t}, \qquad (29)$$

where J_0 denotes the cylindrical Bessel function of order zero; A is the wave magnitude; k_z and k_R are the partial wave numbers in the beam axis (z axis) and transverse direction (R axis), respectively; $R = \sqrt{x^2 + y^2}$; and $k_R = k \sin \gamma$. For this numerical study, we consider a BSW with $\gamma = \pi/3$, at which the transverse and longitudinal wavelengths are comparable and the effects of the nonplanar wave front become relatively significant.

Before studying the particle interactions, it is important to investigate the difference between the effects of PSW and BSW on particles with different material properties in terms of the primary radiation force. Under a PSW, the nodal planes along the wave direction are the particle trapping locations due to the action of the primary force [1,2,8]. While under a zero-order BSW, the particles tend to migrate toward certain rings on the nodal planes. These rings are the intersections of the nodal planes with the cylindrical zero-pressure and zero-velocity surfaces with radii approximately equal to the roots of J_0 and J_1, respectively.

To further investigate the impact of the particle's material, we studied the magnitude of the primary force from BSW and PSW for a wide range of c/c_f and ρ/ρ_f values, as shown in Fig. 7. The primary force is zero in both cases when the particle's material is the same as the host fluid, as marked by (1,1) on the graphs. It was found that there are other combinations of material properties that also give zero primary force. Particles with the density and speed of sound ratios (ρ/ρ_f and c/c_f) that fall below the zero-force line move toward velocity nodes (V.N.). Those with ratios above the zero-force threshold migrate toward the pressure node (P.N.) under both BSW and PSW. Using water as the host fluid, we marked four points for the cases of air bubbles, hexane droplets, solid polystyrene,

and Pyrex spheres, to illustrate particles above and below the zero-force line. In practical applications with water, the range of possible values for density and speed of sound ratios fall within the shaded area. Considering this narrow region from the graph, it was found that there exists some material choices, marked with the white circle on the right panel, that enable the particle to migrate toward the pressure node under BSW, opposite to their behavior of toward velocity node in PSW. These results show that, for some particle materials in a given host fluid, there is a choice of planar or nonplanar standing waves to achieve different outcomes of separating or clustering particles of different material types. The reversal of the primary force component in the wave direction when the external field is changed (from PSW to BSW) shows that the usual formula for contrast factor, Eq. (30c) in Ref. [37], to determine the force direction is limited to cases with plane external field. In the presence of nonplanar field, the normalized force vector S_{pr} should be used as a generalization of the contrast factor that accounts for the shape of the external field.

Next, in Fig. 8, we look at the interaction behavior of a pair of solid spheres at $kR = 0$, 2.78 and 4.42 on the pressure node ($kz = 0$). It is assumed that the source sphere is already at a location where the primary force is zero. By plotting the $[0, s]$ and $[s, s]$ parts of the interaction potential for the probe sphere, we found that the $[s, s]$ contribution is about two to three orders of magnitude smaller than $[0, s]$ contribution, which is similar to the case of PSW. This shows that Eq. (28) provides an accurate approximation of the interaction potential regardless of the profile of the external acoustic field. The interaction force profiles at $kR = 0$ and 4.42 are also similar, differing only in magnitude. These two locations are the stable trapping locations for solid particles, while $kR = 2.78$ is an unstable equilibrium location.

The interaction forces acting on the probe sphere due to the source sphere located at $kz = 0$ and $kR = 0$, 2.78, and 4.42 are shown in Fig. 9. As expected, the interaction force field at $kR = 0$ and 4.42 have similar patterns but different magnitude. At the unstable equilibrium location $kR = 2.78$,
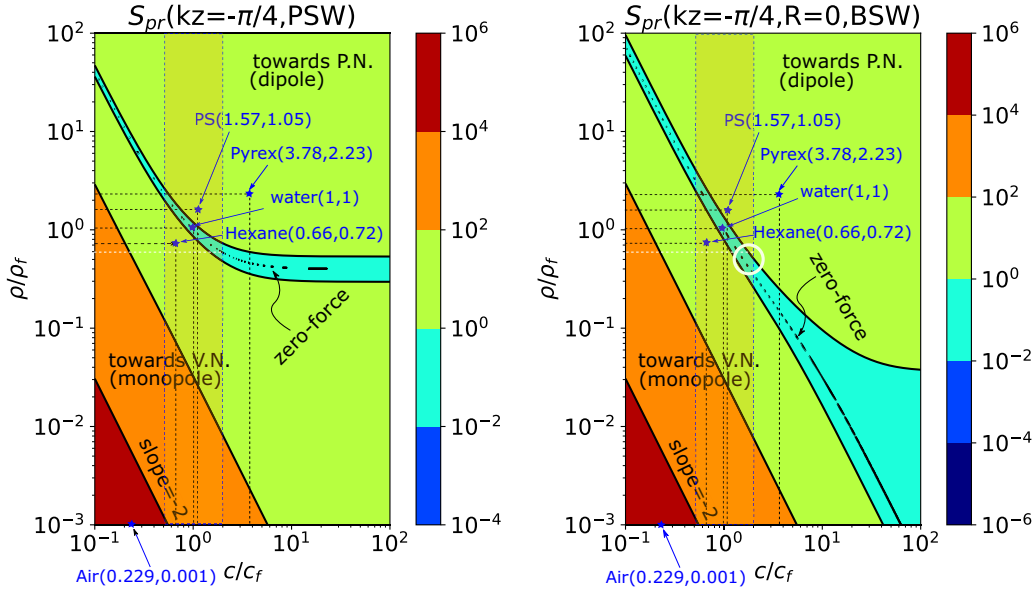
FIG. 7. Contrast factor of the primary force S_{pr} with respect to the material properties of particles at $(kz = \pi/4, R = 0)$, where the force is nonzero and acts only in the wave direction (z axis). The results for PSW and BSW with $\gamma = \pi/3$ are shown in the left and right panels, respectively.

the interaction forces are weaker by at least two orders of magnitude as compared to the fields at $kR = 0$ and 4.42. The x-y projection of the interaction forces at $kR = 0$ and 4.42 shows that the probe particle gets attracted by the source particle from all directions. Whereas, from the x-z projection, it was found that the probe particle tends to migrate to the side of the source particle on the nodal plane due to their close-range interaction. The interaction behavior is more complicated at $kR = 2.78$ since the two spheres could either form

a dumbbell-shaped cluster in x or z direction; nevertheless, such an interaction can be neglected due to the unstable equilibrium at $kR = 2.78$.

Finally, to investigate the balance between the primary and interaction forces acting on the probe sphere, the total acoustic force is plotted in Fig. 10 for the above three locations. In the x-y plane, the interaction force reinforces the primary force in the same direction at $kR = 0$ and $kR = 4.42$, meaning that the probe sphere gets attracted and pushed toward the
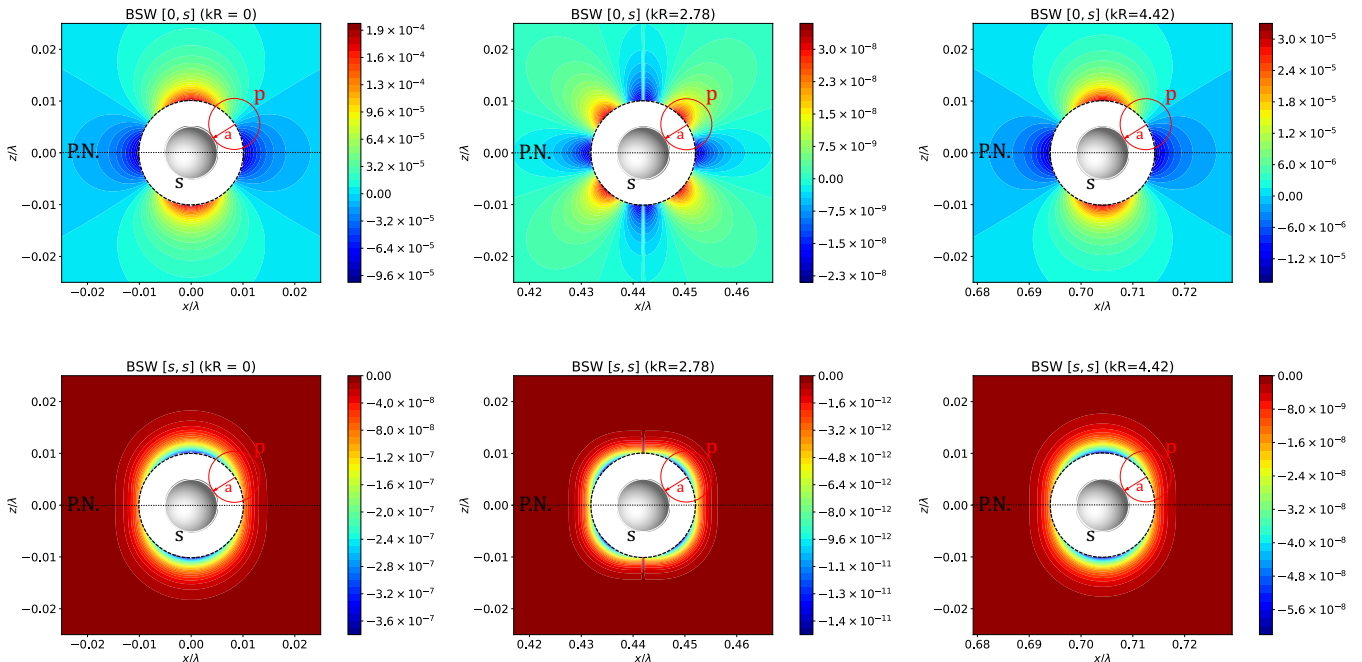

FIG. 8. The $[0, s]$ and $[s, s]$ contributions to the interaction potential under a BSW for a pair of spheres with the source sphere being located at the intersection of the pressure nodal plane at $kz = 0$ and $kR = 0$, 2.78, and 4.42.
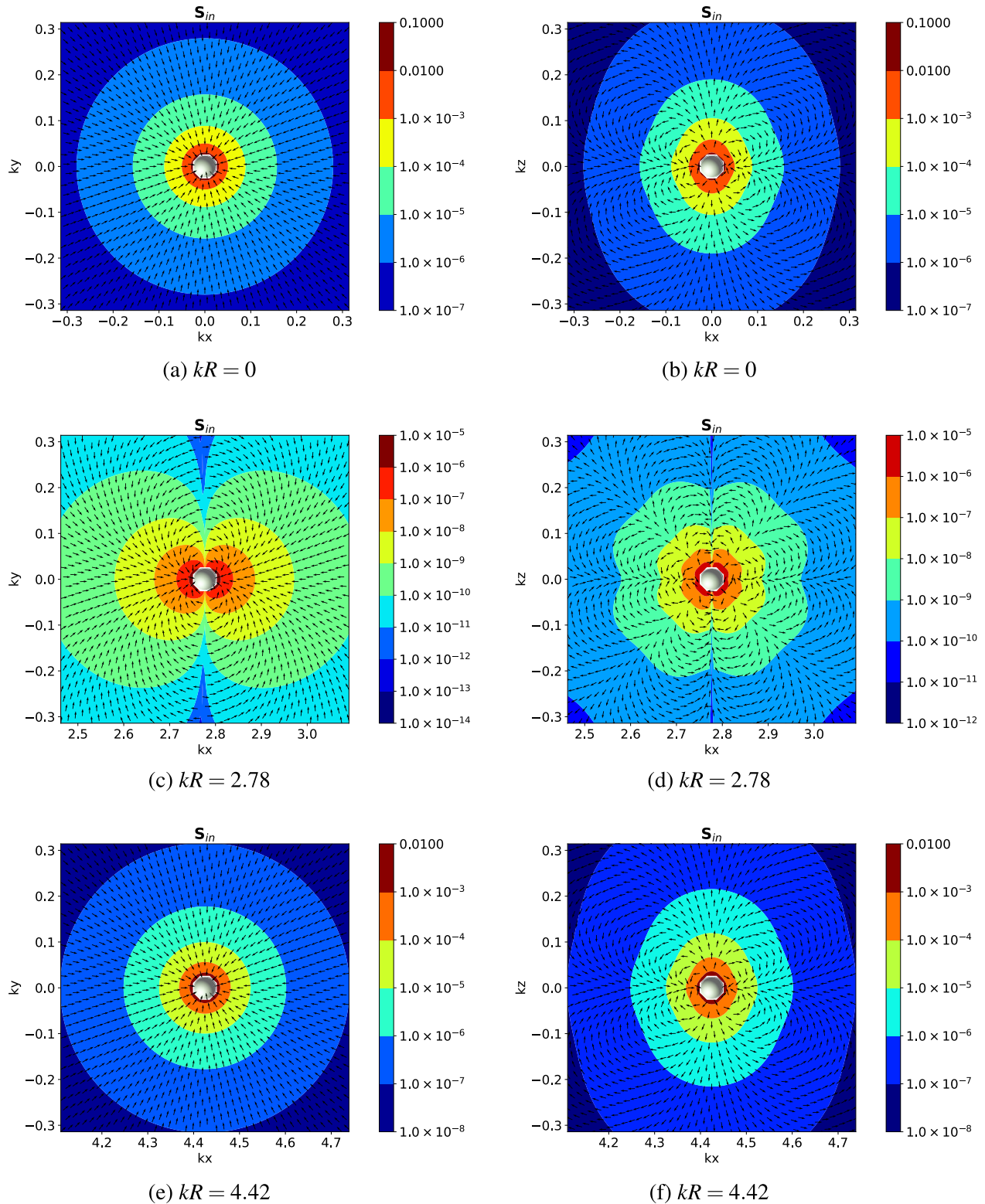
FIG. 9. The *x*-*y* and *x*-*z* projections of the contrast factor of the interaction force under a BSW for a pair of spheres with the source sphere being located at the intersection of the pressure nodal plane at $kz = 0$ and $kR = 0$, 2.78, and 4.42. The vectors length are normalized and their magnitude is shown by the background contours.

source sphere together with the primary force effort. This is not the case at $kR = 2.78$ since the interaction force is in the opposite direction as the primary force; however, it is three orders of magnitude smaller than the primary force and can

be neglected. In the *x*-*z* plane, the interaction force becomes dominant at the vicinity of the source sphere for the two cases of $kR = 0$ and $kR = 4.42$. The probe sphere will be brought to the vicinity of the source sphere by the primary force,
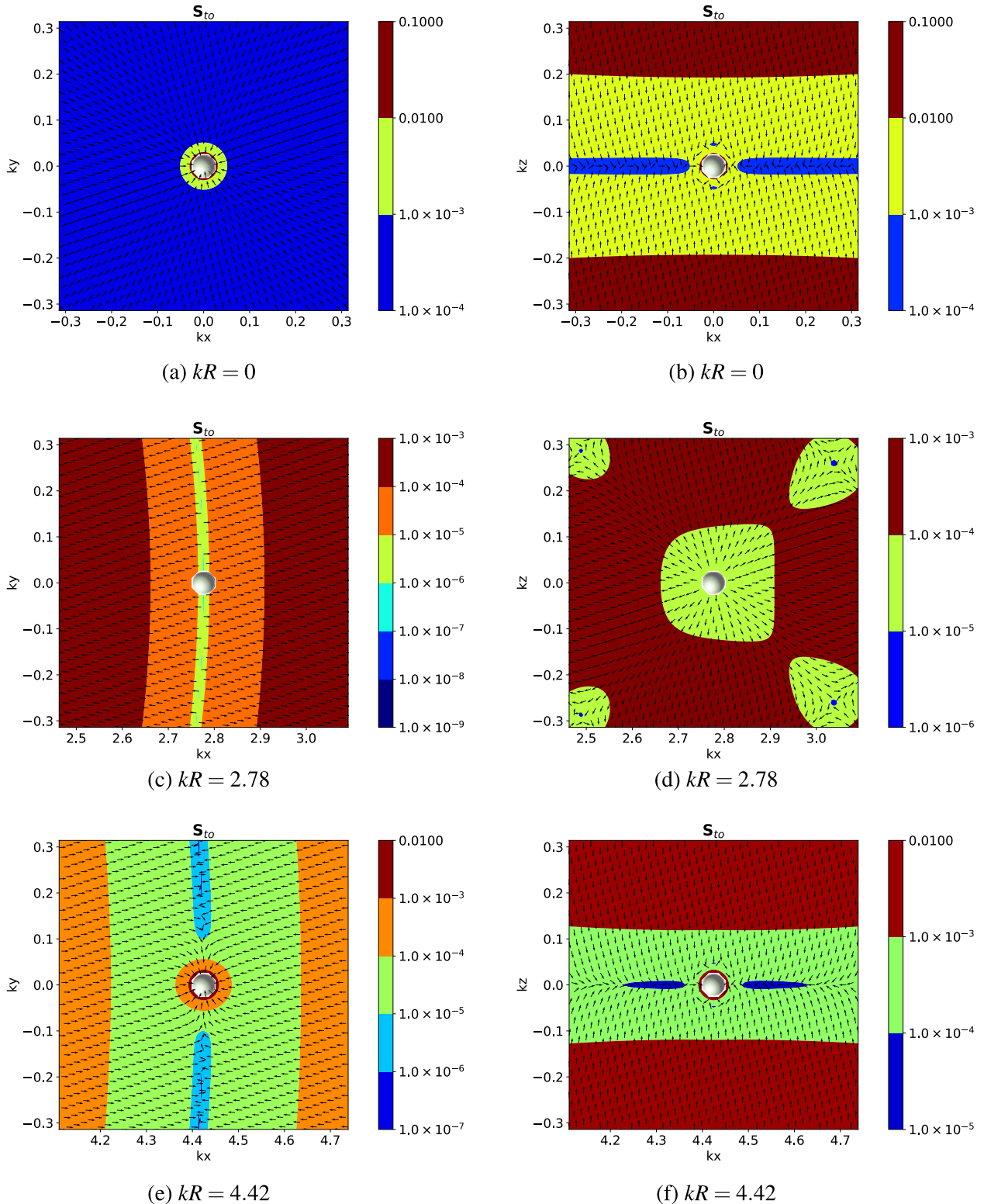
(a) $kR = 0$

(b) $kR = 0$

(c) $kR = 2.78$

(d) $kR = 2.78$

(e) $kR = 4.42$

(f) $kR = 4.42$

FIG. 10. Contrast factor of the total force for a pair of solid spheres with different locations for the source sphere at $kR = 0$, 2.78, and 4.42 on the pressure nodal plane at $kz = 0$. The force vectors are normalized while the background colors show their magnitude.

and then, under the action of the interaction force, it gets attracted and attached to the source sphere to form a dumbbell configuration. At $kR = 2.78$, the interaction force is negligible in the x-z plane, and the primary force is dominant in this unstable equilibrium location.

IV. DISCUSSION

The present formulation is an improvement over the earlier work of Silva and Bruus [19]. In their formulation, the scattered wave was calculated from the external wave, as they
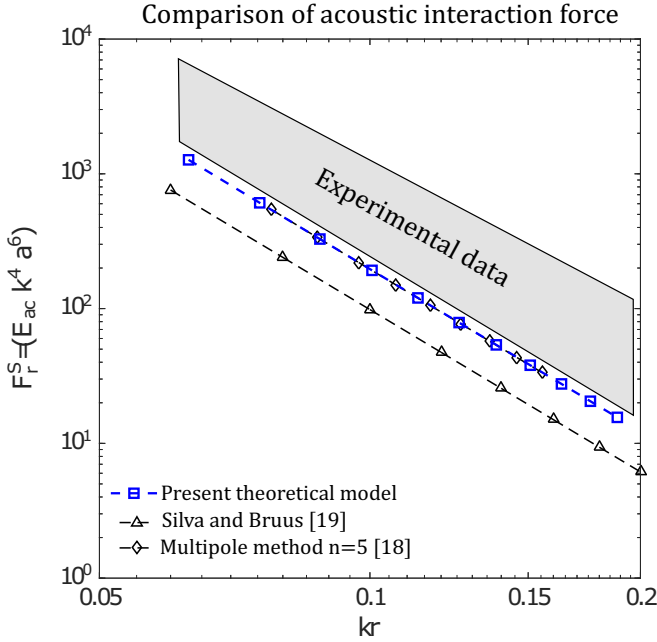
FIG. 11. Comparison of the theoretical estimation of acoustic interaction force for a pair of PS beads in water from the experiments in Ref. [23]. The shaded band shows the area of experimental data points. The results of the present model are shown with a blue dashed line with square markers.

argued that the scattered wave that undergone a single prior scattering of the external wave is dominant. This avoided the need to solve for a fully coupled multibody scattering problem. The formulation in Ref. [19] was also simplified with one dipole coefficient for cases exhibiting symmetry, such as spheres directly opposite the nodal plane. As the spheres approach each other from an arbitrary direction, the full set of dipoles must be used. Also, when the separation between the spheres is small, the scattered field coefficients will interact and a coupled system, such as Eq. (25), needs to be solved to ensure accurate results. It was reported that the estimated force by using the formula in Ref. [19] gives around 50% error for close-range interactions within two diameters of the interacting spheres [23]. Figure 11 shows a comparison of the interaction force results from the present model, indicated by blue dashed line with square markers, with previous results. The experimental measurements in Ref. [23] fall in a band indicated by the shaded area. The present results match well with those obtained from complete multipole series method with the cut-off order of five, confirming that the self-product terms ($[s, s]$) are negligible. These results also fall on the lower edge of the experimental data, while the results from Ref. [19] are lower by 50%.

In the present formulation, the scattered wave is approximated by monopole and dipole coefficients. This formulation could be improved by increasing the number of multipoles in the representation of the scattered potential, which is necessary for larger particles outside of the Rayleigh limit. If one includes the quadrupole terms, then it will increase both the number of coefficients to be solved in the coupled multiscattering problem and the number of terms in the force potential.

Until this idea is formulated mathematically, readers are encouraged to use a direct partial-wave series expansion method for large particles outside of the Rayleigh limit [16,18,20]. A proper convergence study is required to determine the minimum number of terms to evaluate the force accurately using this expansion series.

Our analysis of interaction force field in a PSW showed that a triangle-shaped cluster of three particles is plausible when all are within the nodal plane during agglomeration. This is in addition to the pearl-chain configuration. The likelihood of the triangle-shaped clusters emerging in experiments is high since particles tend to move to the nodal plane first under the strong primary force field before interaction forces become dominant. Therefore, it is expected to observe such two-dimensional (2D) configuration along side with the line formation. However, most of the experimental observations showed the pearl-chain agglomeration in a PSW [23,32,33,39]. This means that there may be additional forces in the fluid domain, which drives particles to line up on the nodal plane. These forces could be generated by weak acoustic fields that emerge from the boundaries of the fluid domain, in addition to the applied PSW. The presence of such secondary acoustic fields was noticed during experimental measurement of the interaction forces [23]. Nonetheless, it is suggested that various types of forces in an acoustophoretic application could be identified by observing the agglomeration patterns and simulating them by using theoretical particle tracing.

V. CONCLUSION

In this study, we presented the formulation for a generalized potential for acoustic radiation forces, including that for interparticle force. By using the generalized potential, the close-range interactions among spheres were investigated in the vicinity of the stable equilibrium locations, where the primary force is negligible. For a general 3D sound field, the normalized force which is a vector quantity should be used to indicate the particle's direction of motion. This is a generalization of the scalar contrast factor used for plane waves. The interaction potential was shown to be dominated by the product of the external field and the scattered fields from other spheres, with the product terms of scattered fields being insignificant. The interaction forces in a heterogeneous population of particles are generally not equal and opposite. Furthermore, based on a three-sphere interaction case under plane standing wave, it was concluded that formation of triangular cluster on the nodal plane is equally likely to the well-known pearl-chain configuration. Both configurations can be expected in practical applications, unless there are other forces that prevent the triangular clustering or the initial arrangement of the spheres was controlled in a certain way.

The nonplanar standing wave may achieve different outcomes (separation or clustering particles of different types of materials) as compared to the plane standing wave, providing an additional parameter for design of acoustofluidic devices. For a plane standing wave, strong acoustic interaction occurs at interparticle distances of within 5 times the sphere diameters; however, for the nonplanar Bessel standing wave, such interaction occurs at much smaller interparticle distances

of around 1.25 times of the sphere diameters. Finally, by analyzing the total force induced by Bessel standing wave, we showed that the interparticle force strongly determines the agglomeration pattern of the spheres as they get closer to each other. The present method of generalized potential is a promising model, providing a simple and insightful method to study the radiation forces in an acoustic field. This method will be useful in applications such as acoustic holography, where a spatially complex sound field is generated and utilized.

[1] L. V. King, On the acoustic radiation pressure on spheres, Proc. R. Soc. Lond. A **147**, 212 (1934).

[2] K. Yosioka and Y. Kawasima, Acoustic radiation pressure on a compressible sphere, Acta Acust. **5**, 167 (1955).

[3] L. P. Gorkov, On the forces acting on a small particle in an acoustical field in an ideal fluid, Sov. Phys. Dokl. **6**, 773 (1962).

[4] A. P. Zhuk, Hydrodynamic interaction of two spherical particles due to sound waves propagating perpendicularly to the center line, Sov. Appl. Mech. **21**, 307 (1985).

[5] A A. Doinikov, Acoustic radiation pressure on a compressible sphere in a viscous fluid, J. Fluid Mech. **267**, 1 (1994).

[6] T. Hasegawa and K. Yosioka, Acoustic-radiation force on a solid elastic sphere, J. Acoust. Soc. Am. **46**, 1139 (1969).

[7] A. A. Doinikov, Acoustic radiation pressure on a rigid sphere in a viscous fluid, Proc. R. Soc. Lond. A **447**, 447 (1994).

[8] M. Settnes and H. Bruus, Forces acting on a small particle in an acoustical field in a viscous fluid, Phys. Rev. E **85**, 016327 (2012).

[9] S. Annamalai, S. Balachandar, and M. K. Parmar, Mean force on a finite-sized spherical particle due to an acoustic field in a viscous compressible medium, Phys. Rev. E **89**, 053008 (2014).

[10] S. Sepehrirahnama, K. M. Lim, and F. S. Chau, Numerical analysis of the acoustic radiation force and acoustic streaming around a sphere in an acoustic standing wave, Phys. Proc. **70**, 80 (2015).

[11] S. Sepehrirahnama, F. S. Chau, and K. M. Lim, Effects of viscosity and acoustic streaming on the interparticle radiation force between rigid spheres in a standing wave, Phys. Rev. E **93**, 023307 (2016).

[12] P. L. Marston, Axial radiation force of a Bessel beam on a sphere and direction reversal of the force, J. Acoust. Soc. Am. **120**, 3518 (2006).

[13] P. L. Marston, Axial radiation force of a Bessel beam on a sphere, direction reversal of the force, and solid sphere examples, J. Acoust. Soc. Am. **121**, 3109 (2007).

[14] P. L. Marston, W. Wei, and D. B. Thiessen, Acoustic radiation force on elliptical cylinders and spheroidal objects in low frequency standing waves, in *AIP Conference Proceedings*, Vol. 838 (AIP, 2006), pp. 495–499.

[15] A. N. Guz and A. P. Zhuk, Hydrodynamic interaction between two spherical particles in an ideal fluid in a sound wave field, in *Doklady Akademiia Nauk SSSR*, Vol. 279 (Akademiia, Moscow, 1984), pp. 566–570.

[16] A. A. Doinikov, Acoustic radiation interparticle forces in a compressible fluid, J. Fluid Mech. **444**, 1 (2001).

[17] A. Garcia-Sabaté, A. Castro, M. Hoyos, and R. González-Cinca, Experimental study on inter-particle acoustic forces, J. Acoust. Soc. Am. **135**, 1056 (2014).

[18] S. Sepehrirahnama, K. M. Lim, and F. S. Chau, Numerical study of interparticle radiation force acting on rigid spheres in a standing wave, J. Acoust. Soc. Am. **137**, 2614 (2015).

[19] G. T. Silva and H. Bruus, Acoustic interaction forces between small particles in an ideal fluid, Phys. Rev. E **90**, 063007 (2014).

[20] J. H. Lopes, M. Azarpeyvand, and G. T. Silva, Acoustic interaction forces and torques acting on suspended spheres in an ideal fluid, IEEE Trans. Ultrason. Ferroelectr. Freq. Contr. **63**, 186 (2016).

[21] F. B. Wijaya, S. Sepehrirahnama, and K. M. Lim, Interparticle force and torque on rigid spheroidal particles in acoustophoresis, Wave Motion **81**, 28 (2018).

[22] F. Mitri, Acoustic attraction, repulsion and radiation force cancellation on a pair of rigid particles with arbitrary cross-sections in 2D: Circular cylinders example, Ann. Phys. **386**, 1 (2017).

[23] A. R. Mohapatra, S. Sepehrirahnama, and K. M. Lim, Experimental measurement of interparticle acoustic radiation force in the Rayleigh limit, Phys. Rev. E **97**, 053105 (2018).

[24] D. Saeidi, M. Saghafian, S. Haghjooy Javanmard, B. Hammarström, and M. Wiklund, Acoustic dipole and monopole effects in solid particle interaction dynamics during acoustophoresis, J. Acoust. Soc. Am. **145**, 3311 (2019).

[25] D. Saeidi, M. Saghafian, S. Haghjooy Javanmard, and M. Wiklund, A quantitative study of the secondary acoustic radiation force on biological cells during acoustophoresis, Micromachines **11**, 152 (2020).

[26] M. X. Lim, A. Souslov, V. Vitelli, and H. M. Jaeger, Cluster formation by acoustic forces and active fluctuations in levitated granular matter, Nat. Phys. **15**, 460 (2019).

[27] P. L. Marston, Radiation force of a helicoidal Bessel beam on a sphere, J. Acoust. Soc. Am. **125**, 3539 (2009).

[28] L. Zhang and P. L. Marston, Geometrical interpretation of negative radiation forces of acoustical Bessel beams on spheres, Phys. Rev. E **84**, 035601 (2011).

[29] F. Mitri, Acoustic radiation force on oblate and prolate spheroids in Bessel beams, Wave Motion **57**, 231 (2015).

[30] K. Melde, A. G. Mark, T. Qiu, and P. Fischer, Holograms for acoustics, Nature **537**, 518 (2016).

[31] P. Mishra, M. Hill, and P. Glynne-Jones, Deformation of red blood cells using acoustic radiation forces, Biomicrofluidics **8**, 034109 (2014).

[32] D. Hartono, Y. Liu, P. L. Tan, X. Y. S. Then, L. Y. L. Yung, and K. M. Lim, On-chip measurements of cell compressibility via acoustic radiation, Lab Chip **11**, 4072 (2011).

[33] A. Lenshof, C. Magnusson, and T. Laurell, Acoustofluidics 8: Applications of acoustophoresis in continuous flow microsystems, Lab Chip **12**, 1210 (2012).

[34] M. Wiklund, Acoustofluidics 12: Biocompatibility and cell viability in microfluidic acoustic resonators, Lab Chip **12**, 2018 (2012).

[35] M. Wiklund, R. Green, and M. Ohlin, Acoustofluidics 14: Applications of acoustic streaming in microfluidic devices, Lab Chip **12**, 2438 (2012).

[36] F. B. Wijaya, A. R. Mohapatra, S. Sepehrirahnama, and K. M. Lim, Coupled acoustic-shell model for experimental study of cell stiffness under acoustophoresis, Microfluid. Nanofluid. **20**, 69 (2016).

[37] H. Bruus, Acoustofluidics 7: The acoustic radiation force on small particles, Lab Chip **12**, 1014 (2012).

[38] H. Bruus, Acoustofluidics 10: Scaling laws in acoustophoresis, Lab Chip **12**, 1578 (2012b).

[39] P. Augustsson, C. Magnusson, M. Nordin, H. Lilja, and T. Laurell, Microfluidic, label-free enrichment of prostate cancer cells in blood based on acoustophoresis, Anal. Chem. **84**, 7954 (2012).